

1 **When does vapor pressure deficit drive or reduce**
2 **evapotranspiration?**

3 **A. Massmann¹, P. Gentine¹, C. Lin²**

4 ¹Department of Earth and Environmental Engineering, Columbia University, New York, NY 10027

5 ²Department of Hydraulic Engineering, Tsinghua University, Beijing, CN

6 **Key Points:**

- 7 • = enter point 1 here =
8 • = enter point 2 here =
9 • = enter point 3 here =

10 **Abstract**

11 = enter abstract here =

12 **1 Introduction**

13 Changes to vapor pressure deficit (VPD) alter the atmospheric demand for water from
 14 the land surface. Traditionally, atmospheric scientists and hydrometeorologists generally
 15 think that an increase in atmospheric demand induces an increases in evapotranspiration
 16 (ET) (citations?). This possible misconception developed in part due to the proliferation of
 17 studies examining potential ET rather than estimates of ET itself (citations?). In contrast, plant
 18 physiologists know that stomata have evolved to optimally regulate the exchange of water
 19 and carbon, and tend to close in response to increased atmospheric dryness [??*MEDLYN*
 20 *et al.*, 2011]. Therefore, an increase (decrease) in VPD may not correspond to an increase
 21 (decrease) in ET because stomatal closure (opening) can cancel the effects of shifts to atmo-
 22 spheric demand.

← This section
needs to be
fleshed out,
and I defi-
nitely need
to add more
citations

23 Quantifying the plant response to a perturbation to atmospheric VPD increases our un-
 24 derstanding of land surface response to shifts in atmospheric conditions. If plant response
 25 reduces ET in response to atmospheric drying then soil moisture will be conserved. An in-
 26 crease in ET in reponse to atmospheric drying will reduce soil moisture, but contribute in-
 27 creased moisenting to the atmosperhere. Clearly, the sign and magnitude of land-surface
 28 responsedrives the co-evolution of the atmosphere and land-surface at many timescales, from
 29 diurna to interdecadal.

30 In order to quantify plant response to perturbations to atmospheric demand for water,
 31 we apply a Penman-Monteith framework to eddy-covariance observation spanning various
 32 biomes and climates. Section 2 describes the data used, Section 3 derives the framework,
 33 Section 4 presents results, and Section 5 discusses conclusions. The goal of this paper is
 34 to use reasonable approximations as a tool to increase intuition for plant response to atmo-
 35 spheric drying. This intuition will aid interpretation of observations and full complexity cli-
 36 mate models.

37 **2 Methods**

38 The Penman-Monteith equation (hereafter PM) estimates ET as a function of atmo-
 39 spheric and land-surface variables:

$$40 \quad ET = \frac{\Delta R + g_a \rho_a c_p D_s}{\Delta + \gamma(1 + \frac{g_a}{g_s})}, \quad (1)$$

41 where variable definitions are given in Table 1. *MEDLYN et al.* [2011] developed a
 42 model for g_s by combining optimal photosynthesis theory with empirical approaches. The
 43 result for leaf-scale stomatal resistance was:

$$44 \quad g_{l-s} = g_0 + 1.6 \left(1 + \frac{g_1}{\sqrt{D_s}} \right) \frac{A}{c_s} \quad (2)$$

45 This can be adapted to an ecosystem-scale stomatal resistance by multiplying by leaf
 46 area index (LAI) and converting units to m s^{-1}

$$47 \quad g_s = \text{LAI} \frac{RT}{P} \left(g_0 + 1.6 \left(1 + \frac{g_1}{\sqrt{D_s}} \right) \frac{A}{c_s} \right) \quad (3)$$

48 While Equation 3 can be used in PM, it will make analytical work with the function
 49 intractable because A is a function of ET itself. To remove dependence of ET on A we can
 50 use the semi-empirical results of *Zhou et al.* [2015]. *Zhou et al.* [2015] showed that:

$$51 \quad uWUE = \frac{GPP \cdot \sqrt{D}}{ET} \quad (4)$$

52 is relatively constant across time and space (within plant functional type). If, following *Lin*
 53 *et al.* [2015], we approximate g_0 as 0, we can use $uWUE$ to remove A from g_s in a way that
 54 makes PM analytically tractable:

$$55 \quad g_s = \frac{RT}{P} 1.6 \left(1 + \frac{g_1}{\sqrt{D_s}} \right) \frac{\sigma uWUE ET}{c_s \sqrt{D}} \quad (5)$$

56 Note that $uWUE$ is fit on the ecosystem scale in *Zhou et al.* [2015] so GPP in 4 is re-
 57 ally $A \cdot \text{LAI}$. We also recognize that our use of $uWUE$ introduces considerable uncertainty,
 58 so we added an uncertainty parameter $\sigma = f(t, \text{site})$ modifying $uWUE$. This will be elabo-
 59 rated on below.

60 Next, plugging Equation 5 into Equation 1 and rearranging gives:

$$61 \quad ET = \frac{\Delta R + \frac{g_a P}{T} \left(\frac{c_p D_s}{R_{air}} - \frac{\gamma c_s \sqrt{D}}{R * 1.6 \sigma uWUE (1 + \frac{g_1}{\sqrt{D}})} \right)}{\Delta + \gamma} \quad (6)$$

62 We can then take the derivative with respect to D to analytically determine ecosystem
 63 response to atmospheric demand perturbations:

$$64 \quad \frac{\partial ET}{\partial D} = \frac{g_a P}{T(\Delta + \gamma)} \left(\frac{c_p}{R_{air}} - \frac{\gamma c_s}{1.6 R * \sigma \text{ uWUE}} \left(\frac{2g_1 + \sqrt{D}}{2(g_1 + \sqrt{D})^2} \right) \right) \quad (7)$$

65 The D dependence in Equation 7 is a little opaque. However, mean D is 1062 Pa, so
 66 \sqrt{D} is 32.6 Pa^{1/2}, which is much less than g_1 (with the exception of ENF; Table 3). So a se-
 67 ries expansion in the limit $\frac{\sqrt{D}}{g_1} \rightarrow 0$ gives an approximation which makes the functional form
 68 more clear:

$$69 \quad \frac{\partial ET}{\partial D} \approx \frac{g_a P}{T(\Delta + \gamma)} \left(\frac{c_p}{R_{air}} - \frac{\gamma c_s}{1.6 R * \sigma \text{ uWUE}} \left(\frac{1}{g_1} - \frac{3\sqrt{D}}{2g_1^2} + \frac{2\sqrt{D}^2}{g_1^3} - \frac{5\sqrt{D}^3}{2g_1^4} + O\left(\left(\frac{\sqrt{D}}{g_1}\right)^4\right) \right) \right) \quad (8)$$

70 Note that given yearly uWUE from Zhou *et al.* [2015], g_1 from Lin *et al.* [2015] [as
 71 presented in Franks *et al.*, 2017], and observations of R, T, P, D_s , and wind speed (WS), all
 72 quantities in Equations 7 and 8 are known except for the uncertainty parameter σ . With flux
 73 tower observations of ET, σ will then be uniquely determined for each observation through
 74 Equation 6:

$$75 \quad \sigma = -\frac{g_a \gamma c_s \sqrt{D_s} P}{(\text{ET}(\Delta + \gamma) - \Delta R - g_a \rho_a c_p D_s) 1.6 R T \text{ uWUE} (1 + \frac{g_1}{\sqrt{D_s}})} \quad (9)$$

76 This σ will be some part uncertainty associated with assumptions about constant g_1
 77 and *uWUE*, including differences between the data used here and in the fits in ? and Lin
 78 *et al.* [2015], but also some general PM model and FLUXNET observational uncertainty.
 79 By calculating a unique σ for each observation we will propagate any model and observa-
 80 tional uncertainty forward into our expression for $\frac{\partial ET}{\partial D}$.

82 3 Data

83 We use data from FLUXNET2015. Because g_1 coefficients [Lin *et al.*, 2015] and *uWUE*
 84 were only both available for five plant functional types (PFTs - see Table 3), only 56 of the 77
 85 sites were used. Figure 1 presents each site and its plant functional type.

86 We restrict our analysis to the daytime (sensible heat > 5 W m⁻¹ and shortwave radia-
 87 tion > 50 W m⁻²) when there is no precipitation and the plants are growing (GPP > 10% of

← map needs
to be im-
proved - it's
a placeholder
for now

81

Table 1. Definition of symbols and variables

| Variable | Description | Units |
|-----------|--|---|
| e_s | saturation vapor pressure | Pa |
| T | temperature | K |
| Δ | $\frac{\partial e_s}{\partial T}$ | Pa K ⁻¹ |
| R | net radiation at land surface minus ground heat flux | W m ⁻² |
| g_a | atmospheric conductance | m s ⁻¹ |
| ρ_a | air density | kg m ⁻³ |
| c_p | specific heat capacity of air at constant pressure | J K ⁻¹ kg ⁻¹ |
| D | VPD | Pa |
| γ | psychrometric constant | Pa K ⁻¹ |
| g_s | stomatal conductance | m s ⁻¹ |
| g_{l-s} | leaf-scale stomatal conductance | mol m ⁻² s ⁻¹ |
| R^* | universal gas constant | J mol ⁻¹ K ⁻¹ |
| LAI | leaf area index | - |
| σ | ratio of LAI to LAI_{ref} in Zhou <i>et al.</i> [2015] | - |
| c_s | CO ₂ concentration | μ mol CO ₂ mol ⁻¹ air |

^aFootnote text here.

86

⁸⁷ **Table 2.** Plant functional types, their abbreviation, Medlyn coefficient [from Lin *et al.*, 2015], and uWfUE
⁸⁸ [from Zhou *et al.*, 2015]. Note that units are converted such that the quantities fit into Equations 1-8 with the
variables in Table 1.

| Abbreviation | PFT | g_1 (Pa ^{0.5}) | uWUE (μ -mol [C] Pa ^{0.5} J ⁻¹ [ET]) |
|--------------|-----------------------------|----------------------------|---|
| CRO | cropland | 183.1 | 3.80 |
| CSH | closed shrub | 148.6 | 2.18 |
| DBF | deciduous broadleaf forest | 140.7 | 3.12 |
| ENF | evergreen needleleaf forest | 74.3 | 3.30 |
| GRA | grassland (C3) | 166.0 | 2.68 |

^aFootnote text here.

93 the 95th percentile) . Also, because some sites use half hourly data but some use hourly, we
94 aggregate all data to hourly averages. Only times with good quality control flags are used.

← This GPP thresholding was used by Changjie, do you know if there is a citation for it? Otherwise it seems like something a reviewer would have issue with as it is arbitrary

95 4 Results

96 By construction, the variability in the σ term (Equation 9) contains all model and ob-
97 servational uncertainties. We expect LAI to be close to LAI_{ref} , so σ should be $O(1)$. We
98 can have some confidence in our framework, including the assumption of constant uWUE,
99 if calculated σ s are generally $O(1)$. Figure 2 presents the histogram of calculated σ s with
100 outliers (lowest and highest 5% percent) and nonphysical values ($\sigma < 0$) removed. All re-
101 maining σ values are $O(1)$ which provides confidence in model framework.

105 An additional concern is that the σ term may in fact be some function of D , in which
106 case the dependence would need to be accounted for when taking the derivative. Figure 3.
107 plots the joint distribution of σ and VPD, and shows that σ is very weakly a function of
108 VPD. Given this weak dependence, we argue that Equation 7 is a valid approximation for
109 ET response to D .

← Figs 2 and 3 can probably be combined - the histogram of σ is shown in Fig 3

114 Before calculating the sensitivity of ET to VPDn, it is useful to consider the functional
115 form of Equation 7. There are three terms: a scaling term for the full expression we will call
116 Term 1 ($\frac{g_a P}{T(\Delta+\gamma)}$), a relatively constant offset we will call Term 2 ($\frac{c_p}{R_{air}}$), and a variable term
117 we will call Term 3 ($\frac{\gamma c_s}{1.6 R \text{ uWUE}} \left(\frac{2g_1 + \sqrt{D}}{2(g_1 + \sqrt{D})^2} \right)$). All variables are positive, so the relative mag-
118 nitude between Term 2 and Term 3 will determine the sign of the derivative, while Term 1
119 will scale the expression larger or smaller.

120 In Term 1, $\frac{P}{T} \propto \rho$, so this should vary little relative to g_a and Δ . γ should also be rel-
121 atively constant, So the scaling term, Term 1, should be primarily a function of g_a and tem-
122 perature (through the function Δ). While temperature range may vary for PFT, the functional
123 form of Δ will be the same. g_a will vary strongly with PFT due to the importance of surface
124 roughness. However, the coefficient of variability for both g_a and Term 1 is relatively con-
125 stant across PFT, suggesting that the influence of g_a on the relative (to the mean) variability
126 of Term 1 is approximately similar across PFT.

127 Figure 4A shows Term 1 normalized by mean g_a (calculated for each plant functional
128 type), and confirms that much of the relative variability of Term 1 is contained in the g_a
129 term's relative variability. Generally, T has less of a role. Additionally, the impact of T on
130 the relative variability increases with increasing g_a .

131 While the relative variability of Term 1 is similar across PFT, the absolute value of
 132 Term 1 varies strongly across PFT. Figure 4B shows Term 1 evaluated with the mean g_a for
 133 each PFT, and at the range of observed temperatures for each PFT. As expected, for the tree
 134 PFTs (DBF, ENF) Term 1 is much larger and the temperature dependence is much stronger.
 135 Systematic differences in observed temperatures also cause differences in the average mag-
 136 nitude of Term 1. For example, ENF experiences on average colder temperatures and is thus
 137 more likely to have a larger scaling term. Additionally, because $\text{std}(g_a) \propto \overline{g_a}$, the spread of
 138 Term 1 due to g_a variability will be larger for the tree PFTs, although this is not shown for
 139 simplicity. To summarize, the variability of Term 1 within each PFT will look like Figure 4A
 140 for each PFT, but the scale of the x and y-axis will increase or decrease according to mean g_a
 141 observed in Figure 4B.

146 Term 2 minus Term 3 determines the sign of the sensitivity of ET to VPD and is thus
 147 crucial. c_s variability is relatively less than σ and D variability, then variability within PFT
 148 will be solely determined by σ and D at the different fluxnet sites. Figure 5 shows how (Term
 149 2 - Term 3) varies with D and σ , as a function of PFT. In Figure 5a lower uWUE and σ
 150 shift the distribution of (Term 2 - Term 3) towards negative values. Additionally, the smaller
 151 g_1 , the greater the relative D dependence of (Term 2 - Term 3). This is observed most
 152 strongly for the ENF PFT, which has the smallest g_1 (74.31).

159 Figure 5b shows the location of the minima of ET, as a function of σ and D . For any σ
 160 or VPD less (more) than these curves, Term 2 - Term 3 will be negative (positive). It is clear
 161 that the portion of VPD observations below/above these curves will be a strong function of
 162 σ . However, we can see some general trends. For CSH, $\frac{\partial ET}{\partial D}$ should be negative for the vast
 163 majority of observed σ and VPD. The fraction of positive $\frac{\partial ET}{\partial D}$ appears to be more even for
 164 ENF, GRA, and DBF, and we might expect a greater frequency of positive $\frac{\partial ET}{\partial D}$ for CRO.

165 Table 3 confirms these expectations for PFT behavior of $\frac{\partial ET}{\partial D}$. For all PFTs except for
 166 CRO, average $\frac{\partial ET}{\partial D}$ is less than zero. However, $\frac{\partial ET}{\partial D}$ evaluated at the average of all variables
 167 (e.g. σ , T , c_s , D) is only negative for CSH and GRA. And, DBF in addition to CRO experi-
 168 ences $\frac{\partial ET}{\partial D} < 0$ less than half the time. These observations highlight the effect of the nonlin-
 169 ear function in Figure 5: $\frac{\partial ET}{\partial D}$ has a much steeper slope when the function is negative, and is
 170 thus more likely to be large.

171 The units of $\frac{\partial ET}{\partial D}$ make it difficult to interpret if D is even a meaningful contributor to
 172 ET's variability. To better understand D 's contribution, we normalize $\frac{\partial ET}{\partial D}$ with D 's standard

192

Table 3. Statistics of $\frac{\partial ET}{\partial D}$ as a function of PFT.

| PFT | $\frac{\partial ET}{\partial VPD}$ | $\overline{\frac{\partial ET}{\partial D}}(\overline{T}, \dots, \overline{D})$ | $\overline{\frac{\partial ET}{\partial D}}(\overline{T}, \dots, \overline{D}) * std(D)$ | $\frac{\overline{\frac{\partial ET}{\partial D}}(\overline{T}, \dots, \overline{D}) * std(D)}{\overline{\frac{\partial ET}{\partial R}}(\overline{T}, \dots, \overline{D}) * std(R)}$ | fraction $\frac{\partial ET}{\partial VPD} < 0$ |
|-----|------------------------------------|--|---|---|---|
| CRO | 0.000853 | 0.026241 | 18.523659 | 0.203022 | 0.473311 |
| CSH | -0.108234 | -0.091526 | 50.861613 | 0.439379 | 0.931660 |
| DBF | -0.012727 | 0.013794 | 19.734435 | 0.164241 | 0.461674 |
| ENF | -0.034087 | 0.000706 | 16.611852 | 0.148548 | 0.534425 |
| GRA | -0.019637 | -0.000921 | 16.798083 | 0.173552 | 0.631735 |

^aFootnote text here.

173

deviation to define a (linearized) relative change in ET for variations in D . D 's contribution to ET's variability ranges between 16 - 20 W m⁻² for all PFTs except for CSH, which is about 51 W m⁻². Another meaningful comparison is to $\frac{\partial ET}{\partial R} * std(R)$, as net radiation is generally the driver of ET (cite joe berry here). For all PFTs except for CSH D contributes between 14.5 - 20.5 % of R 's contribution to variability. For CSH the portion is much larger, about 44 %. D 's variability is certaintly a non-negligable contributor to ET 's variability.

179

So far, idealized plots and statistics have illuminated the form of $\frac{\partial ET}{\partial D}$ and how it varies with PFT. Large mean σ and uWUE shifts CRO and DBF towards positive $\overline{\frac{\partial ET}{\partial D}}$. However, the strongly nonlinear function of $\frac{\partial ET}{\partial D}$ at $\frac{\partial ET}{\partial D} < 0$ pushes $\overline{\frac{\partial ET}{\partial D}}$ negative for DBF (it does not do this for CRO because of CRO's high $g1$). ENF's low $g1$ value increases the dependence of $\frac{\partial ET}{\partial D}$ on D , and makes the function more strongly nonlinear. This has the side effect of pushing $\overline{\frac{\partial ET}{\partial D}}$ negative further than other PFTs for a given fraction $\frac{\partial ET}{\partial D} < 0$ and magnitude $\frac{\partial ET}{\partial D}(\overline{T}, \dots, \overline{D})$. GRA shows the opposite behavior; a relatively high $g1$ makes the function more linear, decreasing the magnitude of $-\overline{\frac{\partial ET}{\partial D}}$ for a given [large] fraction $\frac{\partial ET}{\partial D} < 0$ and negative $\frac{\partial ET}{\partial D}(\overline{T}, \dots, \overline{D})$ (although g_a and Term 1 also probably have a role in this). Finally, low uWUE of CSH pushes to toward by far the lowest values $\frac{\partial ET}{\partial D}$ (Figure 5). Variability in D accounts for the largest about of ET variability for CSH. For the other PFTs, D contributes less to ET variability, but still represents about 15-20 % of R 's contributions to ET variability.

174

175

176

177

178

179

180

181

182

183

184

185

186

187

188

189

190

191

193 **4.1 Full observations of $\frac{\partial ET}{\partial D}$**

194 Now that we have an intuitive understanding of $\frac{\partial ET}{\partial D}$'s behavior, we are equipped to
 195 interpret fully realistic plots of $\frac{\partial ET}{\partial D}$ for each PFT. Figure 6 presents calculated $\frac{\partial ET}{\partial D}$ where,
 196 unless otherwise noted, all variables in Equation 7 are allowed to vary. Each column is a
 197 different quantity related to $\frac{\partial ET}{\partial D}$, and each row is a different PFT.

198 The full observations generally confirm expectations from Section 4. CRO has the
 199 most positive values of $\frac{\partial ET}{\partial D}$, $\frac{\partial ET}{\partial D}$ is almost always negative for CSH, and response depends
 200 more with the environmental conditions for the other PFTs (especially ENF). Through the
 201 columns of Figure 6 we can see the impact of σ and g_a on the variability of $\frac{\partial ET}{\partial D}$. g_a 's scal-
 202 ing (included in columns 1 and 3) alters the magnitude considerably. σ variability (included
 203 in columns 1 and 2) adds a lot of additional noise to the signal of $\frac{\partial ET}{\partial D}$, which is slightly un-
 204 desirable given σ 's role in representing model and observational uncertainty. However, the
 205 general story with the noise appears to match the cleaner signal when σ is help constant and
 206 D_{ETmin} is clearly visible . One exception is possibly with GRA, for which uncertainty repre-
 207 sented in σ is high and causes the full complexity plots (Columns 1 and 2) to not match well
 208 with σ held fixed (Columns 3 and 4).

← I really need
to make
these plots
better - way
too much
overlapping
of points
that hurts the
story

209 For ENF and GRA D_{ETmin} does not appear to be only a function of σ (most observ-
 210 able in Column 4). It turns out that the site to site variability in γ causes D_{ETmin} to vary,
 211 which is not discussed in the previous section. The impact is observable in both ENF and
 212 GRA, but especially for ENF which has a larger $\frac{\partial^2 ET}{\partial^2 D}$ than the other PFTs.

213 In general the full complexity plots of $\frac{\partial ET}{\partial D}$ match our expectations, even with the large
 214 sensitivity to σ measures of uncertainty observed in Figure 5. Our σ -based method of un-
 215 certainty propagation blurs the idealized expectations the most for GRA, and also has a con-
 216 siderable effect for CRO. We therefor have the most confidence in our conclusion based on
 217 Equation 7 for PFTS CSH, DBF, and ENF, as the full complexity plots with uncertainty in-
 218 cluded closely match the story when σ is held fixed. **see somewhat preferred alternate
 219 figure 7 .

← I think I like
the alternate
plot much
more as
thinking in
terms of T
and RH is
easier, and
it makes the
story easier
to see at rel-
atively low
temperatures.
However,
I used the
other plot be-
cause Fig 5
does not dis-
cuss things
in terms of

220 **5 Conclusions**

221 The idealized representation of ET used here is successful in developing intuition for
 222 how ET responds to changes in D . This intuition will aid the community in interpreting ob-
 223 servations and output from sophisticated full complexity climate models.

232 The idealized framework leads to the following general conclusions:

- 233 • Aerodynamic resistance plays an important role of scaling $\frac{\partial ET}{\partial D}$. This is a leading
234 order effect for observing higher magnitude responses in DBF and ENF.
- 235 • In general, CSH has the most negative (i.e. ET reduced) response to increases in D
236 (atmospheric drying). So CSH plants will almost always try and conserve water, ef-
237 fectively reducing ET with dry atmospheric perturbation.
- 238 • Additionally for CSH, D variability contributes the most to ET variability.
- 239 • CRO has the most positive response (i.e. ET increased) in response to increases in
240 D . This is consistent with CROs that may be evolved or bred to thrive in non-water-
241 limited environments.
- 242 • The response is more a function of the environment for DBF, ENF, and GRA. Be-
243 cause as VPD increases the response is more likely to be positive, if RH is fixed then
244 the response will be more likely to be positive at warmer T, or if T is fixed the re-
245 sponse is more likely to be positive with decreasing RH.
- 246 • ENF has the strongest dependence on environmental conditions due to its small g_1 .
- 247 • Model and observational uncertainty is highest for GRA and CRO, so conclusions
248 about those PFTs should be tempered.
- 249 • However, inclusion of uncertainty doesn't alter conclusions about DBF, ENF, and
250 CSH.

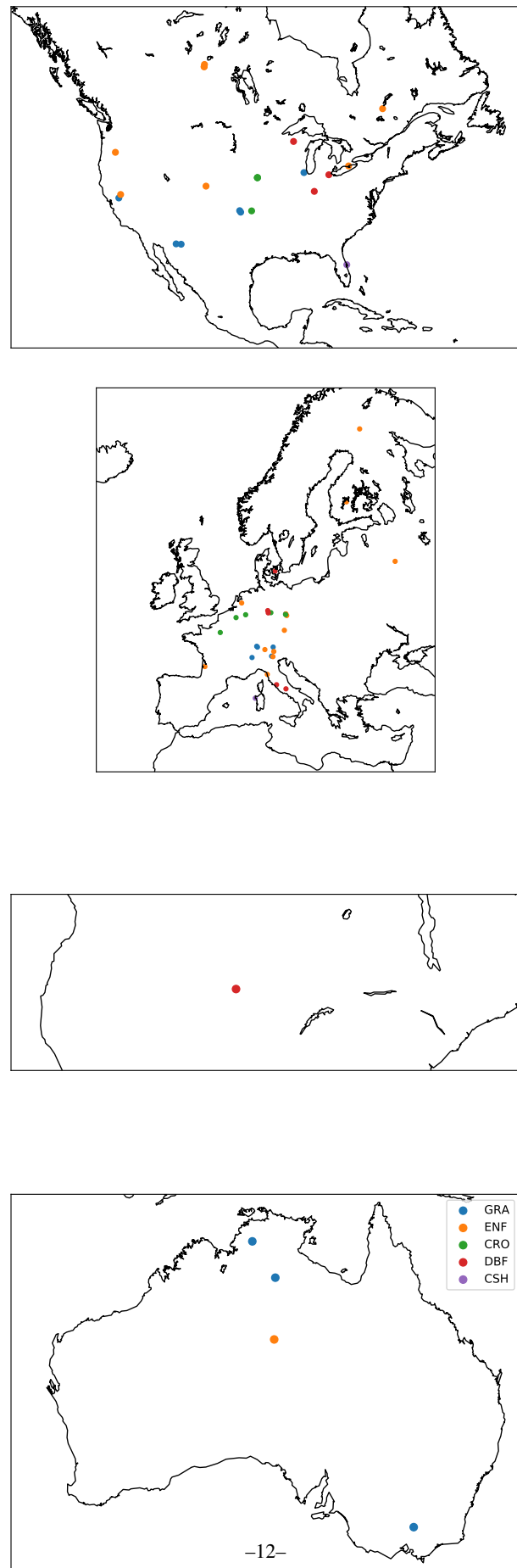
251 The intuition developed using this framework can be used to understand how the land
252 surface will respond and contribute to changes in the environment.

253 Acknowledgments

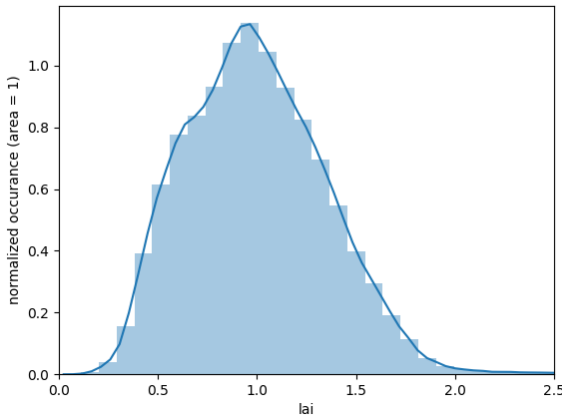
254 This work used eddy covariance data acquired and shared by the FLUXNET community, in-
255 cluding these networks: AmeriFlux, AfriFlux, AsiaFlux, CarboAfrica, CarboEuropeIP, Car-
256 boItaly, CarboMont, ChinaFlux, Fluxnet-Canada, GreenGrass, ICOS, KoFlux, LBA, NECC,
257 OzFlux-TERN, TCOS-Siberia, and USCCC. The ERA-Interim reanalysis data are provided
258 by ECMWF and processed by LSCE. The FLUXNET eddy covariance data processing and
259 harmonization was carried out by the European Fluxes Database Cluster, AmeriFlux Man-
260 agement Project, and Fluxdata project of FLUXNET, with the support of CDIAC and ICOS
261 Ecosystem Thematic Center, and the OzFlux, ChinaFlux and AsiaFlux offices.

References

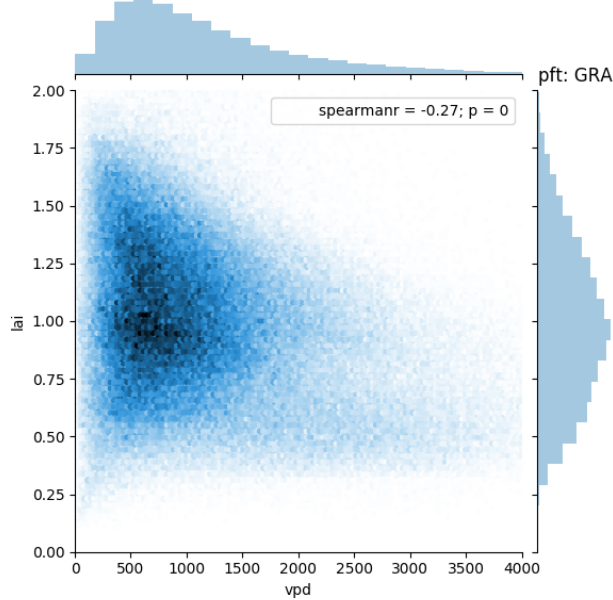
- 262 Franks, P. J., J. A. Berry, D. L. Lombardozzi, and G. B. Bonan (2017), Stomatal function
263 across temporal and spatial scales: Deep-time trends, land-atmosphere coupling and
264 global models, *Plant Physiology*, 174(2), 583–602, doi:10.1104/pp.17.00287.
- 265 Lin, Y.-S., B. E. Medlyn, R. A. Duursma, I. C. Prentice, H. Wang, S. Baig, D. Eamus, V. R.
266 de Dios, P. Mitchell, D. S. Ellsworth, M. O. de Beeck, G. Wallin, J. Uddling, L. Tarvainen,
267 M.-L. Linderson, L. A. Cernusak, J. B. Nippert, T. W. Ocheltree, D. T. Tissue, N. K.
268 Martin-StPaul, A. Rogers, J. M. Warren, P. D. Angelis, K. Hikosaka, Q. Han, Y. Onoda,
269 T. E. Gimeno, C. V. M. Barton, J. Bennie, D. Bonal, A. Bosc, M. LÃºw, C. Macinins-
270 Ng, A. Rey, L. Rowland, S. A. Setterfield, S. Tausz-Posch, J. Zaragoza-Castells, M. S. J.
271 Broadmeadow, J. E. Drake, M. Freeman, O. Ghannoum, L. B. Hutley, J. W. Kelly,
272 K. Kikuzawa, P. Kolari, K. Koyama, J.-M. Limousin, P. Meir, A. C. L. da Costa, T. N.
273 Mikkelsen, N. Salinas, W. Sun, and L. Wingate (2015), Optimal stomatal behaviour
274 around the world, *Nature Climate Change*, 5(5), 459–464, doi:10.1038/nclimate2550.
- 275 MEDLYN, B. E., R. A. DUURSMA, D. EAMUS, D. S. ELLSWORTH, I. C. PRENTICE,
276 C. V. M. BARTON, K. Y. CROUS, P. D. ANGELIS, M. FREEMAN, and L. WINGATE
277 (2011), Reconciling the optimal and empirical approaches to modelling stomatal conduc-
278 tance, *Global Change Biology*, 17(6), 2134–2144, doi:10.1111/j.1365-2486.2010.02375.x.
- 279 Zhou, S., B. Yu, Y. Huang, and G. Wang (2015), Daily underlying water use efficiency for
280 AmeriFlux sites, *Journal of Geophysical Research: Biogeosciences*, 120(5), 887–902, doi:
281 10.1002/2015jg002947.



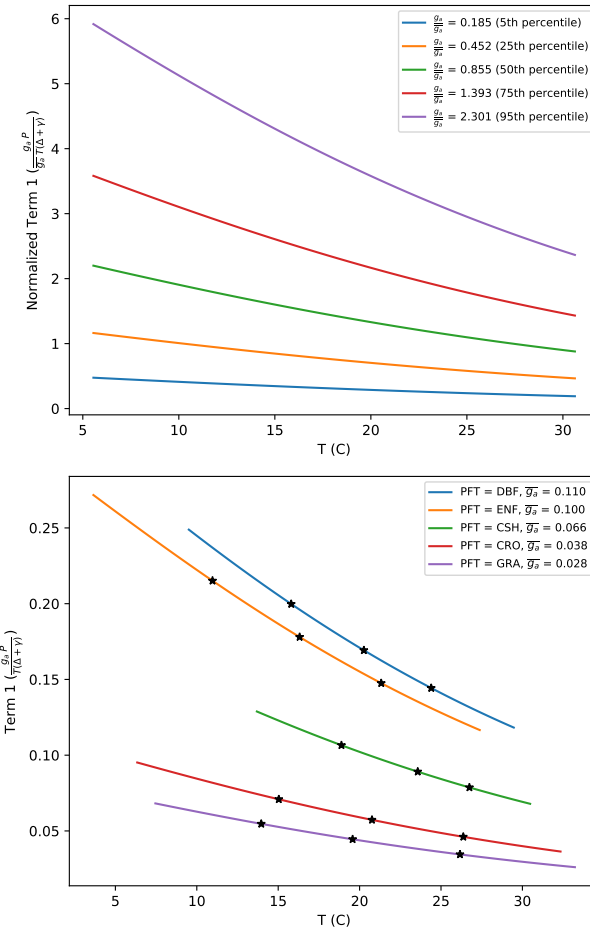
89 **Figure 1.** Plant functional type and location of sites used in analysis. ***This is just a placeholder for now
90 and needs to be improved i.e. with lat lon, better placement of continents, etc.)***



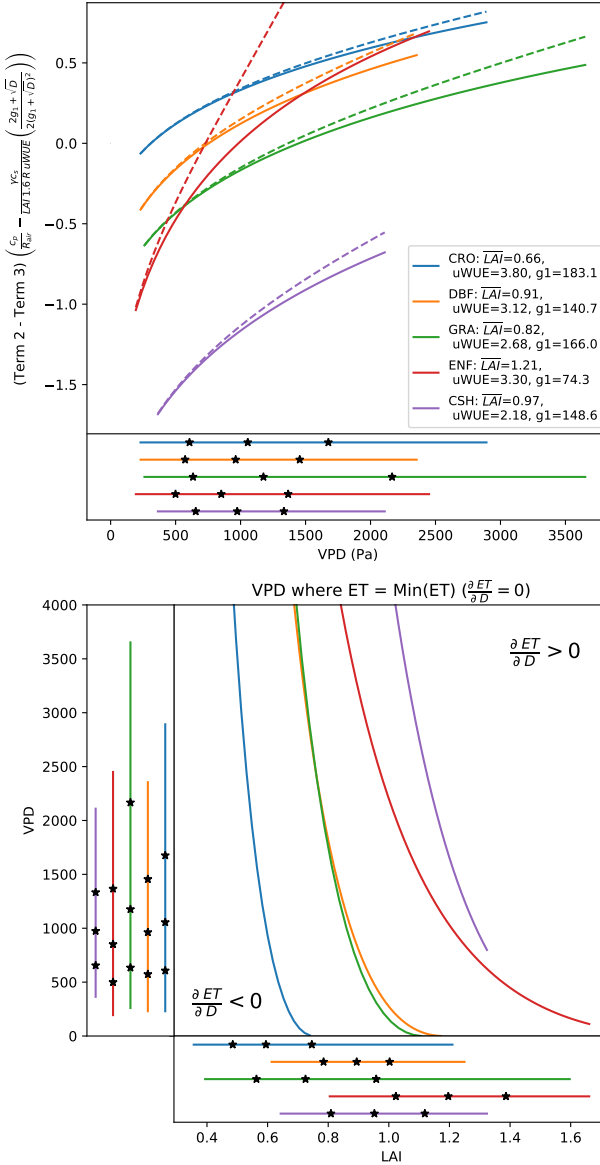
102 **Figure 2.** Histogram of σ values calculated for each site and time according to Equation 9.
 103 The lowest and highest 5% are removed as outliers, as well as any values below 0.
 104 The curve is normalized such that its area is 1.



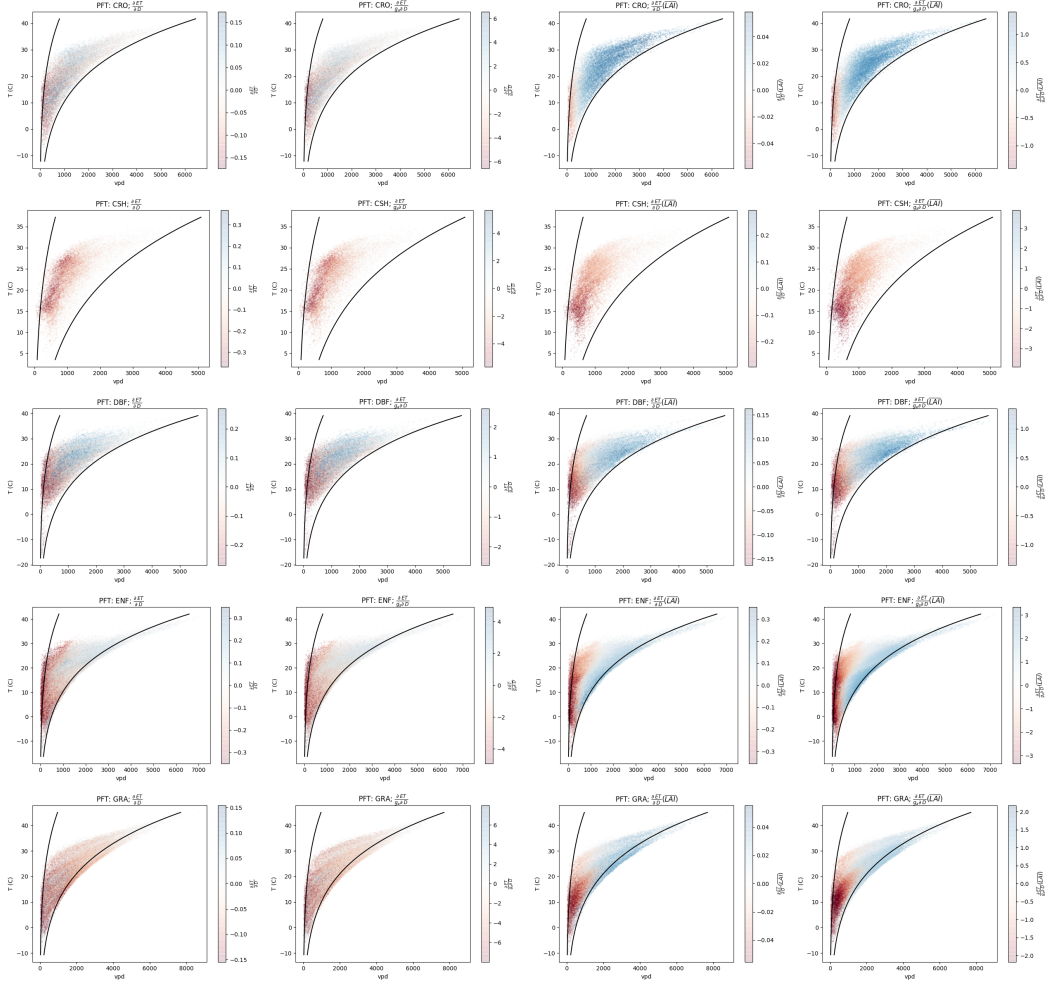
110 **Figure 3.** The joint distribution of D and σ . σ has only a weak dependence on D . ***This plot could
 111 probably benefit from a box plot of site specific correlations, because some sites do have stronger depen-
 112 dence than others. Note also Figs 3 and 2 can probably be combined because this figure shows σ 's his-
 113 togram.***



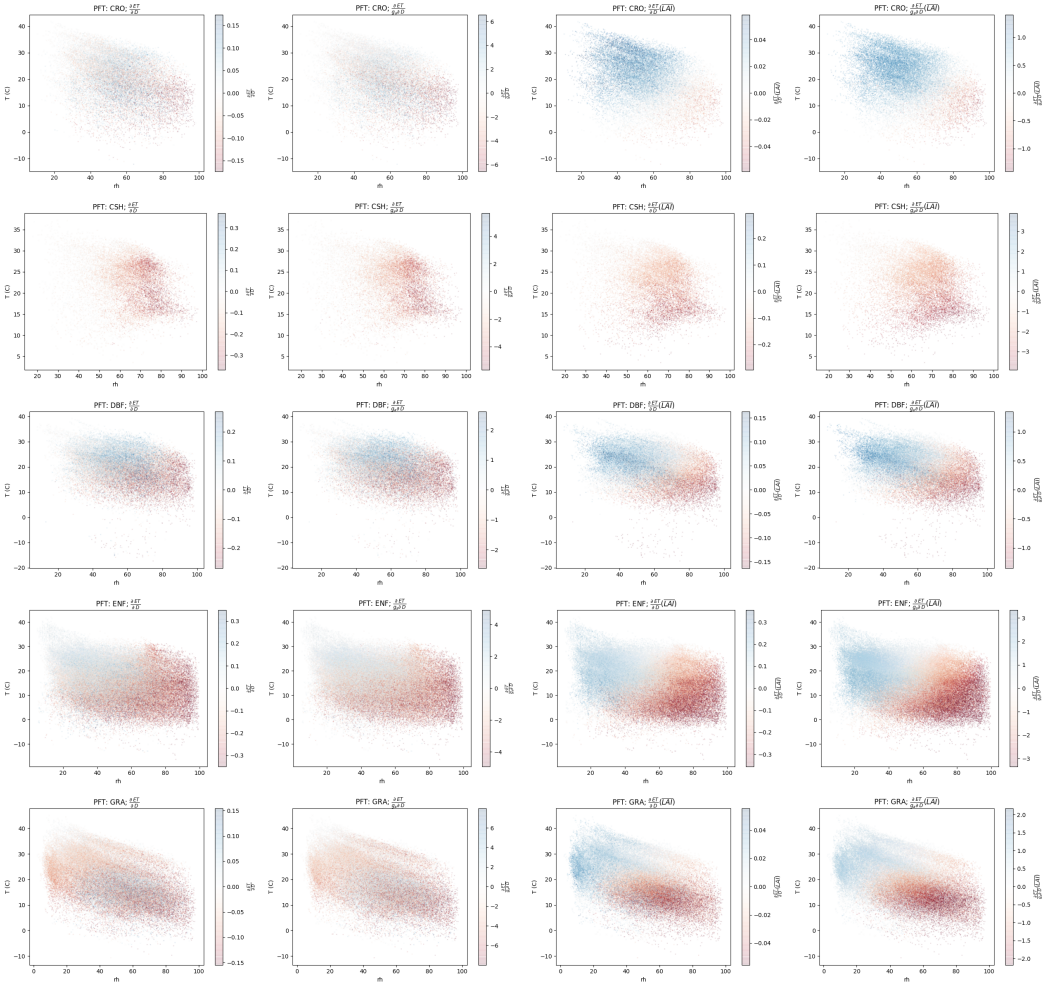
142 **Figure 4.** Primary sources of variability for Term 1. A) Variability within each PFT: Term 1 normalized by
 143 mean g_a for each PFT. B) Variability between each PFT: Term 1 evaluated at mean g_a for each PFT. Tempera-
 144 ture range is 5-95th percentile for each PFT. Additionally, stars denote the location of the 25th, 50th, and 75th
 145 percentiles.



153 **Figure 5.** Sources of variability for Term 2 - Term 3. Top: Term 2 - Term 3 as a function of VPD, with σ
 154 held fixed at PFT averages. The observed range of VPD for each PFT is also shown below the x-axis. Line
 155 extent corresponds to 5th and 95th percentiles, while stars denote the location of the 25th, 50th, and 75th
 156 percentiles.
 157 Bottom: The location of the minima of ET, as a function of VPD and σ . Lines and stars denote the distribu-
 158 tion of VPD and σ next to each axis, following the same percentiles as above.



213 **Figure 6.** Scatter plots of $\frac{\partial ET}{\partial D}$. Each row is a different PFT, and each column is a different quantity related
 214 to $\frac{\partial ET}{\partial D}$, as labeled: Column 1 - $\frac{\partial ET}{\partial D}$; Column 2 - $\frac{\partial ET}{\partial D}$ normalized by g_a ; Column 3 - $\frac{\partial ET}{\partial D}$ with σ held
 215 fixed at PFT average; and Column 4 - $\frac{\partial ET}{\partial D}$ normalized by g_a and with σ held fixed. For reference, lines
 216 corresponding to RH = 20% and RH = 90 % are drawn. Please note differences in the colorbar scale. ***see
 217 alternate (or additional) plot below.***



225 **Figure 7.** ****alternate Fig 06**** Scatter plots of $\frac{\partial ET}{\partial D}$. Each row is a different PFT, and each column
 226 is a different quantity related to $\frac{\partial ET}{\partial D}$, as labeled. If I end up using this, I could also draw on the curve of
 227 D_{ETmin} with $\overline{\text{LAI}_{ref}}$.